PNNL-11568
UC-2040

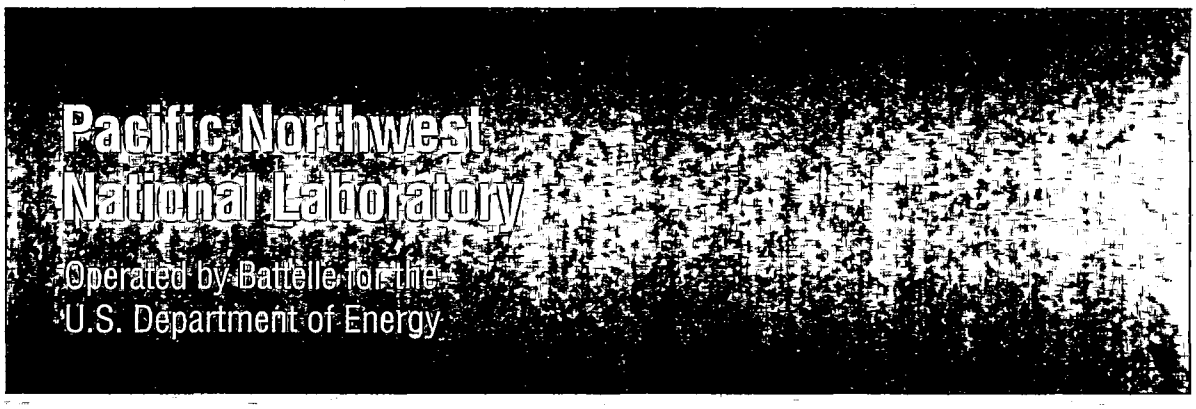

Treatment Studies of Plutonium-Bearing INEEL Waste Surrogates in a Bench-Scale Arc Furnace

C. J. Freeman

May 1997

Prepared for the U.S. Department of Energy
under Contract DE-AC06-76RLO 1830

PNNL-11568

DISCLAIMER

PACIFIC NORTHWEST NATIONAL LABORATORY
operated by
BATTELLE
for the
UNITED STATES DEPARTMENT OF ENERGY
under Contract DE-AC06-76RLO 1830

Printed in the United States of America

Available to DOE and DOE contractors from the Office of Scientific and Technical Information, P.O. Box 62, Oak Ridge, TN 37831; prices available from (615) 576-8401.

Available to the public from the National Technical Information Service, U.S. Department of Commerce, 5285 Port Royal Rd., Springfield, VA 22161

The document was printed on recycled paper

PNNL-11568
UC-2040

Treatment Studies of Plutonium-Bearing INEEL Waste Surrogates in a Bench-Scale Arc Furnace

C. J. Freeman

May 1997

Prepared for
the U.S. Department of Energy
under Contract DE-AC06-76RLO 1830

Pacific Northwest National Laboratory
Richland, Washington 99352

Summary

Since 1989, the Subsurface Disposal Area (SDA) at the Idaho National Environmental and Engineering Laboratory (INEEL) has been included on the National Priority List for remediation. Arc- and plasma-heated furnaces are being considered for converting the radioactive mixed waste buried in the SDA to a stabilized-vitreous form. Nonradioactive, surrogate SDA wastes have been melted during tests in these types of furnaces, but data are needed on the behavior of transuranic (TRU) constituents, primarily plutonium, during thermal treatment. To begin collecting this data, plutonium-spiked SDA surrogates were processed in a bench-scale arc furnace to quantify the fate of the plutonium and other hazardous and nonhazardous metals. Test conditions included elevating the organic, lead, chloride, and sodium contents of the surrogates. Blends having higher organic contents caused furnace power levels to fluctuate. An organic content corresponding to 50% INEEL soil in a soil-waste blend was the highest achievable before power fluctuations made operating conditions unacceptable.

The glass, metal, and off-gas solids produced from each surrogate blend tested were analyzed for elemental (including plutonium) content and the partitioning of each element to the corresponding phase was calculated. In each test, the metal phase partitioning values for plutonium were nearly identical to those for calcium, aluminum, and titanium, with the highest and lowest values measured at 6.0% and 0.1%, respectively. The presence of plutonium in the metal was concluded to be primarily from glass contaminating the samples. In each test, the partitioning values for plutonium, to the off-gas solids phases, ranged from 0.3% to 2.0%. These values were also nearly identical to those for calcium, aluminum, and titanium. Because of the low vapor pressure of plutonium and each of these other elements' oxide forms, entrainment, not volatilization, was concluded to be the mechanism for their transfer to the off-gas. The analyses for chromium and lead partitioning revealed that less than one half of the chromium and one quarter of the lead for each surrogate blend partitioned to the metal phases, and less than 8% of the chromium and between 25% and 60% of the lead partitioned to the off-gas.

Contents

Figures

Tables

Acknowledgments

Pacific Northwest National Laboratory is operated for the U.S. Department of Energy by Battelle under Contract DE-AC06-76RLO 1830. The work reported here was supported by the U.S. Department of Energy's EM-50 Landfill Stabilization Focus Area and Mixed Waste Focus Area programs.

Introduction

Between 1952 and 1972, low-level and transuranic (TRU) wastes were buried in shallow pits and trenches at the Subsurface Disposal Area (SDA) in the Idaho National Environmental and Engineering Laboratory's (INEEL) Radioactive Waste Management Complex (RWMC). Based on the Comprehensive Environmental Response, Compensation, and Liability Act (CERCLA) decision process, INEEL's SDA has been on the National Priority List for remediation since 1989 (Geimer et al. 1992). Since then, remediation strategies have identified thermal treatment of the SDA buried wastes to produce a stabilized-vitreous form as a highly rated option (Mayberry et al. 1991). Systems being considered for this type of treatment include arc- and plasma-heated furnaces.

The high temperatures produced by arc- and plasma-heated furnaces (>2000°C) enable the pyrolization or combustion of hazardous and nonhazardous organic constituents. Additionally, inorganic waste constituents can be melted into either a durable glass or a metal product with relative volumes far less than the starting waste material. Furthermore, the glass product can immobilize hazardous and radioactive constituents for subsequent disposal. In recent years, testing has been performed in arc- and plasma-heated furnaces of various scales with surrogate SDA wastes. These tests were primarily performed without radioactive constituents in the surrogates. As a result, little data are available on the behavior of TRU constituents, namely plutonium, during thermal treatment. Thus, the focus of the present work is the treatment of plutonium-spiked SDA surrogates in an arc-heated furnace. The fates of plutonium, as well as other hazardous and nonhazardous metals, are quantified for the treatment of several surrogate variations. This data will provide some of the information needed about the products and secondary waste streams from larger thermal treatment systems to permit implementation of such systems.

Description of SDA Waste

Characterization of SDA buried waste has identified a wide variety of materials (Bonnenberg et al. 1993). Ten million cubic feet (290,000 m^3) of soil at the SDA are potentially contaminated with radioactive and hazardous constituents (Nickelson et al. 1992). Many wastes are buried in steel drums and cardboard boxes. Waste materials include construction and demolition materials (e.g., lumber, bricking, asphalt, concrete), decontamination materials (e.g., rags, plastic bags) and maintenance equipment (e.g., power tools, oils and grease). Table 1 shows a nominal composition of the SDA wastes used in the present study. Note that this composition does not include any contaminated INEEL soil as its amount within the buried waste can vary.

INEEL soil is primarily composed of SiO_2 (60%), Al_2O_3 (11%), Fe_2O_3 (4%), and CaO (4%). The amount of soil in the SDA waste can be substantial. Temperatures exceeding 1500°C can be required to melt those high-soil compositions into a glassy product. The addition of one part lime (CaO) to approximately 3.1 parts INEEL soil reduces the overall melting temperature of the final glass to as low as 1300°C. For this reason lime has been added to most of the SDA surrogates tested in thermal treatment systems. Note that the notations for each SDA waste surrogate are based on a lime-free composition. For example, a nominal composition of 50% INEEL soil in a soil-waste blend is referred to as Nom-50. However, once lime is added to this mixture, soil content decreases to 43%.

Table 1. SDA Nominal Waste Composition, Without Soil

Organic Constituents:	*(wt %)*	*Master Mix Constituents:*	*(wt %)*
Neoprene	15.5	Micro-Cel (calcium silicate)	5.7
Polyvinylchloride (PVC)	9.7	Water	4.9
Polyethylene (PE)	6.3	Texaco regal oil	3.7
Wood	2.5	Diatomite	3.7
		$NaNO_3$	2.7
Sub-Total =	34.0	KNO_3	1.3
		Portland Cement	1.2
Metallic Constituents:	*(wt %)*	$Al(OH)_3$	1.1
Carbon Steel	22.5	$Fe(OH)_3$	1.1
Stainless Steel	11.5	$Mg(OH)_2$	0.79
Aluminum Metal	1.9	KOH	0.74
Zirconium Metal	0.89	$Ca(OH)_2$	0.66
Copper Metal	0.60	Wheel-bearing grease	0.44
Lead Metal	0.15	NaCl	0.15
		Na_2SO_4	0.15
Sub-Total =	37.6	NaOH	0.15
		Sub-Total =	28.4
		Total =	100.0

The SDA waste surrogate variations tested were Nom-30, Nom-40, Nom-45, and Nom-50. Additionally, variations of metallic lead, PVC, and sodium hydroxide were tested for the Nom-50 material. Those variations were 75, 2, and 2.5 times the respective baseline levels. Table 2 shows the analyzed elemental compositions of each material tested.

The sum of the elemental contents for each test blend in Table 2 totals between 45% and 50%. The remaining mass is primarily organic material. Additionally, the corresponding anions for many of the elements constitute a large portion of the unaccounted-for mass. The plutonium concentration in each blend was held constant at 50.5 nCi per gram. The source of plutonium was plutonium nitrate in an aqueous solution. The predominant isotopes in this source, on a mass basis, were Pu-239 (93%) and Pu-240 (6.6%). On an activity basis, Pu-241 was the predominant species in the mixture (82%) with significant amounts of Pu-239 (14.3%) and Pu-240 (3.7%). Americium in the source was less than 1% on both a mass and activity basis. The specific activity of the isotope mixture was 0.35 Ci per gram.

Table 2. Analyzed Compositions of Nominal SDA Blends Tested (weight percent)

Element	Nom-30	Nom-40	Nom-45	Nom-50	Nom-50 (75XPb)	Nom-50 (2XPVC)	Nom-50 (2.5XNa)
Al	3.28	3.47	3.56	3.65	3.48	3.49	3.51
Ca	8.32	9.80	10.5	11.3	10.7	10.8	10.8
Ce	0.27	0.27	0.27	0.27	0.26	0.26	0.26
Cr	1.12	0.93	0.84	0.75	0.72	0.72	0.73
Fe	19.6	16.7	15.3	13.9	13.2	13.3	13.3
K	1.45	1.45	1.45	1.44	1.37	1.38	1.39
Mg	0.62	0.67	0.68	0.70	0.67	0.67	0.68
Mn	0.07	0.07	0.07	0.07	0.06	0.06	0.06
Na	0.94	0.93	0.92	0.91	0.86	0.87	2.97
Ni	0.88	0.73	0.66	0.59	0.56	0.56	0.57
Pb	0.11	0.09	0.08	0.07	4.73	0.07	0.07
S	0.15	0.12	0.11	0.10	0.10	0.10	0.10
Si	9.75	11.6	12.5	13.4	12.8	12.8	12.9
Ti	0.14	0.17	0.18	0.20	0.19	0.19	0.19
Pu (nCi/g)	50.5	50.5	50.5	50.5	50.5	50.5	50.5
Total	**46.7**	**47.0**	**47.1**	**47.3**	**49.7**	**45.3**	**47.6**

Materials and Methods

Equipment Description

Figure 1 shows the arc furnace system. This system is located in a radiation area within one of Hanford's nuclear facilities. Figure 2 shows a schematic of this system. The furnace uses a single top-entering graphite electrode (cathode) and a fixed graphite hearth (anode). The electrode is 1.5 cm in diameter and can be vertically adjusted using a motor-driven screw. The graphite hearth is crucible shaped; both its internal diameter and its height are 11 cm. A bottomless ceramic crucible is placed inside the graphite hearth during testing to protect the sides from oxidation. The small size of the hearth does not make it amenable to glass and metal drains. Consequently, the furnace is operated in a semi-batch mode, where it is continuously fed until full of molten product, then cooled and disassembled to remove the glass and metal phases produced. The outside of the furnace consists of a stainless steel cylindrical vessel lined with approximately 10 cm of refractory and insulation.

A 15-kW, constant-current DC power supply provides up to 100V of arcing potential between the furnace electrode and hearth during operation. A thermocouple in the furnace plenum area monitors temperature inside the furnace during operation. This temperature, along with the off-gas temperatures,

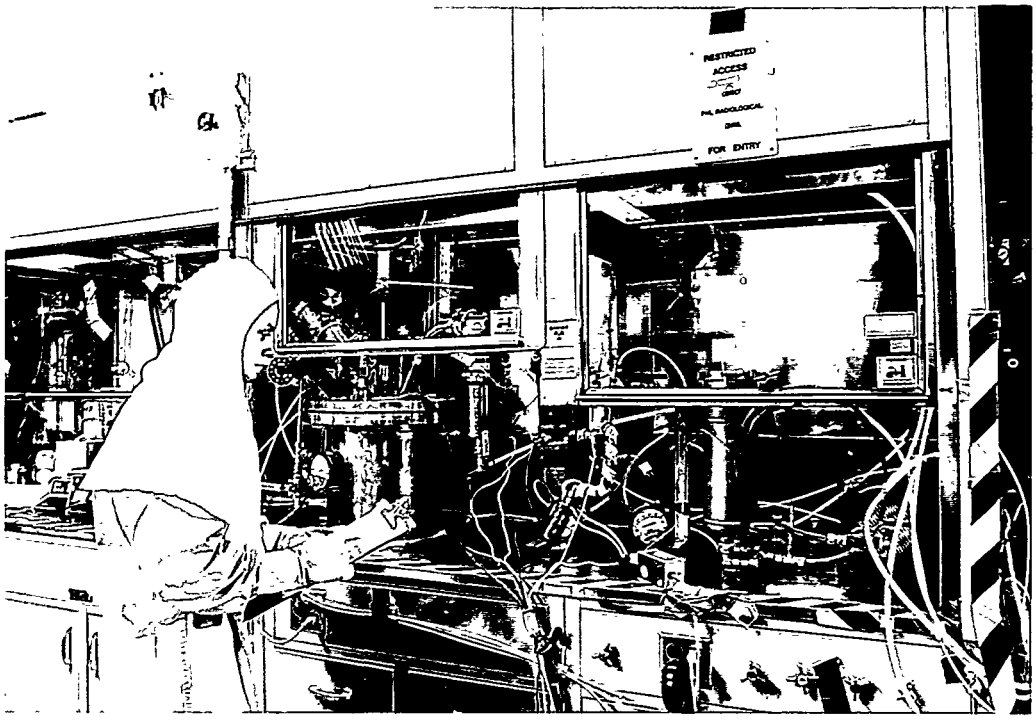

Figure 1. Photograph of the Arc-Heated Furnace Test System

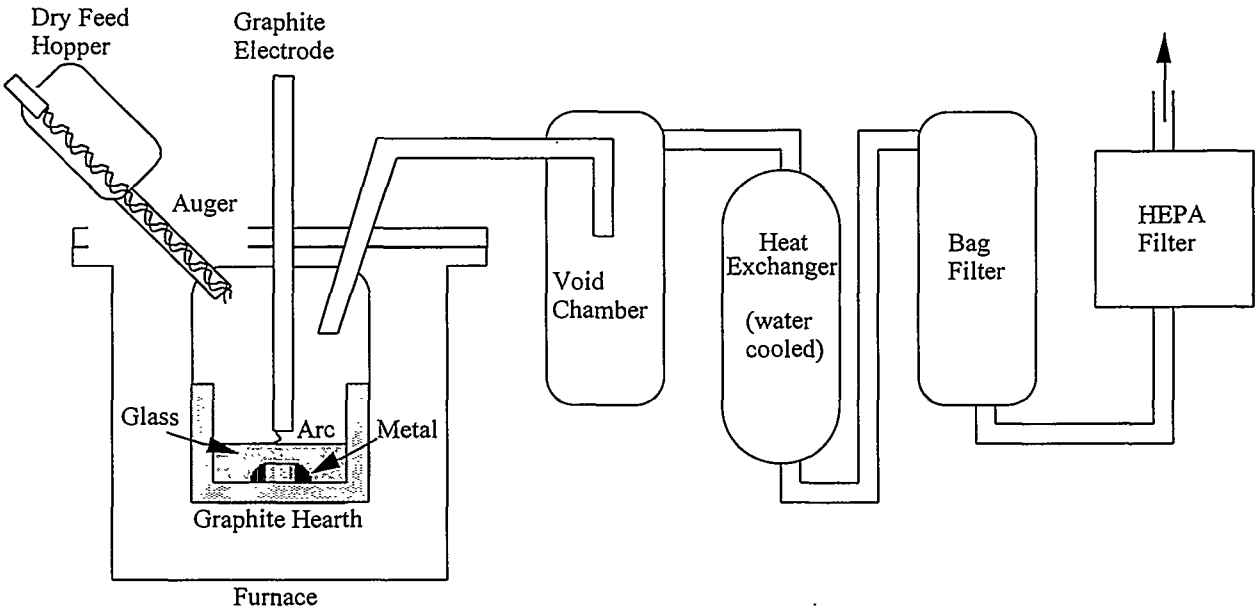

Figure 2. Schematic of the Arc-Heated Furnace Test System

power supply voltage, and current, is electronically logged by a PC-based data acquisition system. As depicted in Figure 2, dry material is fed into the furnace via a screw auger. The auger is driven by a variable speed motor which allows the operator to adjust the feed rate during testing. On-line feed rates cannot be measured from the system. Therefore, feed rates are calculated after each test by dividing the total mass of the feed batch by the amount of time required to feed that batch.

Off-gases exit the furnace and enter a large void chamber where gas velocities are decreased to allow large particulate to settle. The gases next pass through a water-cooled heat exchanger, then through one of two 0.5-μm (absolute) polyester bag filters. In front of the bag filter, the temperature of the off-gas is increased to approximately 80°C using heat tape wrapped around the tubing to ensure that little or no water condenses in the bag filter. Behind the bag filter, the off-gas flows through a high efficiency particulate air (HEPA) filter. All of these components can be completely dismantled so that the entire mass of off-gas solids produced can be collected, weighed, and analyzed. Previous attempts at isokinetically sampling the off-gas solids from such a small system revealed large sources of error in the final carryover determinations.

Experimental Method

Approximately 750 g of surrogate blend were prepared for each test. The individual constituents of each surrogate blend were passed through a 24 mesh sieve so they would mix uniformly. Next, 10 g of surrogate blend were combined with plutonium nitrate solution and heated to 100°C for 30 min. The dried product was then returned to the rest of the surrogate and shaken vigorously to distribute the plutonium. Finally, the surrogate was added to the feed auger.

The arc furnace was started and operated at a current of approximately 100 amps. The potential was adjusted to a target range of 20 to 30 V by varying the electrode position. Feed was added once the furnace plenum temperature reached 500°C. During a given run, the voltage would spike or fluctuate occasionally. An occasional loss of the furnace arc was normal. When arc loss occurred, the electrode was lowered, then raised again to restart the arc. During each test, the furnace vacuum was maintained at 5 cm of water column at a final target off-gas flow rate of 1.4 SCMH. Nitrogen was purged into the furnace at approximately 0.5 SCMH to reduce oxidation of the graphite components. The balance of the gas entering the furnace was air due to inleakage.

After each test, the furnace was dismantled and the solid phases collected, weighed, and sampled. The glass was sampled by breaking the cooled melt and selecting six pieces from different locations from the melt's center. Those pieces were then combined and ground together with a mortar and pestle to provide the sample for analysis. The glass sample preparation followed ASTM procedure C1317-95, using either a Na_2O_2 or KOH fusion. Depending on the fusion salt used, the respective sodium or potassium jeopardized its corresponding analytical value. Each test produced a large metal button at the bottom of the glass melt that was sampled by chopping it into small pieces with bolt cutters. The metal samples were prepared for analysis by dissolving them in a boiling 50% HCl solution for approximately 2 hours.

The removed solids from the off-gas system void chamber, piping, and heat exchanger were combined and weighed, and a sample prepared for analysis using ASTM procedure C1317-95. Similarly, the bag filters were shaken to remove any loose solids, which were prepared and analyzed in the same manner. The bag filters themselves were not analyzed because the presence of aluminum, iron, sodium, silicon, and titanium was discovered in prepared bag filter blanks. These species were unexpected since the bag filters were known to primarily be composed of polyester. An inert matrix within the filter medium or on an exterior coating of the filters is the expected source of these constituents. The error from not analyzing the filters is expected to be minimal since the masses of the loose solids removed from the filters were far more significant than any residual solids on the filters.

All the prepared samples were analyzed by inductively-coupled plasma atomic emission spectroscopy (ICP-AES) for metal concentration. Additionally, each sample was analyzed using zinc sulfide scintillation counting to measure its total alpha activity, or plutonium concentration.

Operational Performance

The data gathered for each test included the masses of feed surrogate, glass, metal, and off-gas solids; run time; feeding time; and power consumption. Table 3 summarizes this information. Additionally, plots of the power, voltage, and plenum temperature for each run are shown in Appendix A. Each of the masses shown in Table 3 have a respective accuracy of ±1 gram. Approximately the same mass of material was fed in each test, except in the Nom-30 test. The glass phases produced in each test were black and amorphous, much like natural obsidian. Additionally, the metal from each test predominantly accumulated in a contiguous button underneath the glass phase. Figure 3 is a photograph of the glass and metal layers produced during a typical test. All of the tests produced light, black, off-gas solids which could be easily knocked out of the off-gas system components by tapping with a hammer. Most of these solids collected in the off-gas system piping and heat exchanger, with small amounts in the void chamber and bag filters.

Each test had an average power consumption, shown in Table 3, of approximately 2.5 kW. Despite these consistent power levels, some feed materials processed with more fluctuations in arc potential than others. These fluctuations were more pronounced in the feed materials with higher organic contents, i.e., Nom-30 and Nom-40. For those tests, the arc potentials fluctuated violently enough to affect the vacuum within the furnace plenum. The rapid expansion of gases resulting from the high-voltage arcs is assumed to have caused these fluctuations in furnace vacuum. The standard deviation of the power consumption was included in Table 3 to help quantify these variations. Figure 4 shows a plot of this value versus feed organic content for each test.

Table 3. Summary of Furnace Testing

	Nom-30	Nom-40	Nom-45	Nom-50	Nom-50 (75XPb)	Nom-50 (2XCl)	Nom-50 (2.5XNa)
Feed Data:							
Mass of Material Fed to System (grams)	521	674	684	618	659	693	687
Operational Data:							
Total Testing Time (min)	188	257	210	227	230	230	230
Total Feeding Time (min)	169	216	206	181	216	216	216
Average Feed Rate (g/min)	3.2	3.1	3.3	3.4	3.1	3.2	3.2
Average Power Consumed (kW)	2.3	2.4	2.5	2.3	2.7	2.8	~2.8
Standard Dev. of Power Consumed (kW)	0.96	0.79	0.66	0.58	0.74	0.79	---
Average Operating Potential (V)	32	29	27	27	35	33	~35
Post-test Data:							
Mass of Metal Product (grams)	78	144	103	67	101	105	98
Mass of Glass Material (grams)	227	314	358	346	348	341	379
Mass of Off-Gas Solids (grams)	25	41	27	11	65	44	42

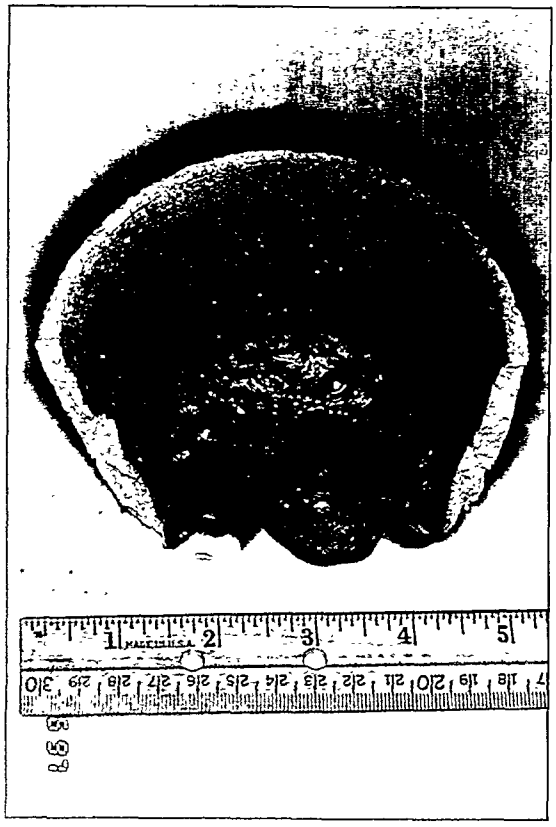

Figure 3. Nom-40 Glass and Metal Furnace Products

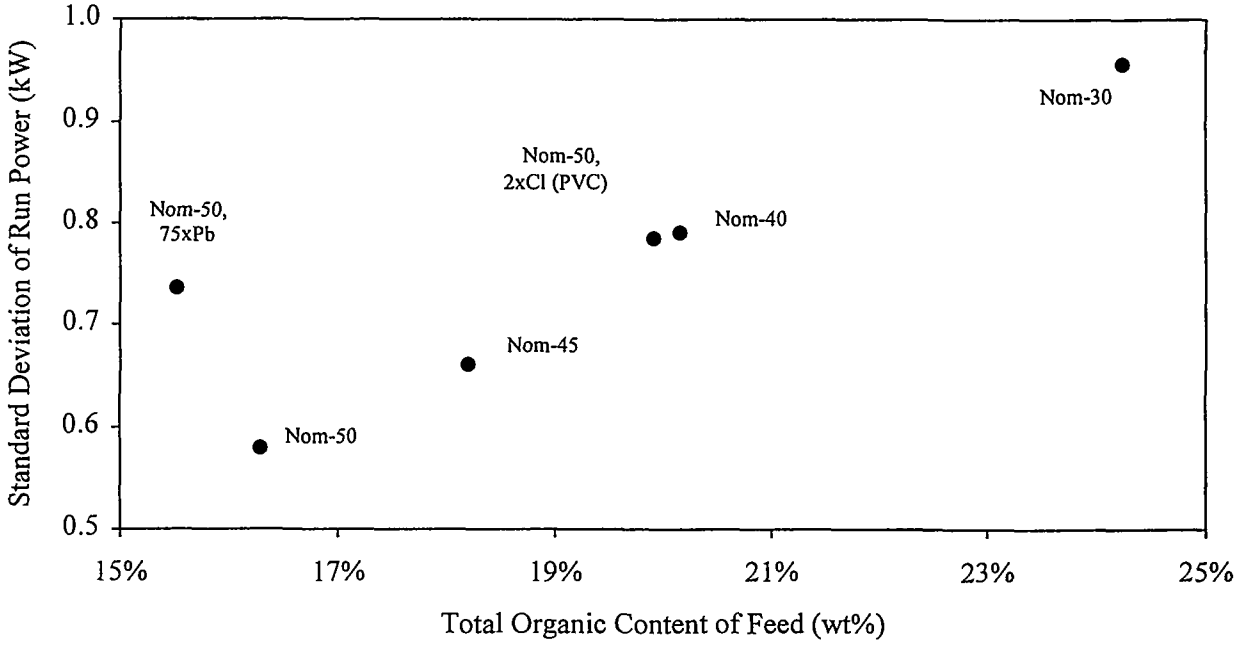

Figure 4. Run Power Standard Deviation Versus Feed Organic Content

Figure 4 shows a definite increase in run power standard deviation with increasing organic content in the feed. While the products from the tests with the Nom-30, Nom-40, Nom-45, and Nom-50 feed materials appeared to be acceptable, Nom-50 represented the lowest average soil content at which the system would still perform acceptably. Subsequent tests were performed with Nom-50. Note that the Nom-50 test with elevated lead also showed an increase in the run power standard deviation. That increase is assumed to be a result of volatilized lead in the arcing regions of the furnace.

Analytical Results

The ICP-AES analytical results for the glass, metal, and off-gas samples for each test are summarized in Tables 4, 5, and 6, respectively. The accuracy of each value is ±10% of the values shown. Recall that the total mass of each phase for each test was given in Table 3. The glasses produced from each test were assumed to be composed of metal oxides. Therefore, Table 4 shows values for an assumed oxide form of each metal.

Table 4 shows the sum of the oxide concentrations to be between 72% and 94%. These totals should be close to 100%; values significantly less than 100% indicate a failure to account for some of the material in the sample. Indeed, tests showing the highest totals also have higher analyzed SiO_2 values. The glass sample preparations are suspected as the source of the lower SiO_2 levels. The glass sample fusions often left a small white solid precipitate in the final solution. These types of precipitates are commonly found to be silica. Indeed, if the silica values in the glass phase are adjusted to the feed levels, the glass oxide percentage totals increase to 90% or higher for each test.

The metal phase concentrations in Table 5 reveal that the metal produced from each test was primarily composed of iron and smaller amounts of nickel. The metal phase elemental totals are nearly 100% for each of the tests, indicating that all of the metal masses were accounted for with reasonable accuracy. The off-gas solid phase concentrations in Table 6 show elemental concentration totals between 15% and 60% for the tests. The balance of the mass in those phases is assumed to be oxygen anion as well as carbon. Carbon is assumed to be present in substantial quantities as indicated by the black color of the off-gas solids.

Table 4. Analyzed Glass Phase Concentrations (wt %) for Each Test

Elemental Oxide	Nom-30	Nom-40	Nom-45	Nom-50	Nom-50 (75XPb)	Nom-50 (2XCl)	Nom-50 (2.5XNa)
Al_2O_3	16.8	14.6	14.1	13.1	10.9	14.0	10.7
CaO	26.2	28.4	26.3	26.9	29.0	27.2	25.9
CeO_2	0.89	0.73	0.32	0.59	0.46	0.00	0.25
Cr_2O_3	2.07	1.87	1.34	1.16	1.50	0.69	1.49
Fe_2O_3	0.84	0.59	0.68	1.00	0.76	0.52	0.99
K_2O	0.29	< 0.33		0.49			
MgO	2.29	2.10	1.62	2.00	1.89	1.84	1.67
MnO	0.20	0.13	0.15	0.16	0.19	0.12	0.16
NiO	0.06	0.08		0.07			
PbO	< 0.04	< 0.08	< 0.11	< 0.08	< 0.29	< 0.07	< 0.13
SO_3	0.29	0.32	0.39	0.41	< 0.66	0.27	< 0.30
SiO_2	36.2	43.8	31.1	46.0	35.2	22.2	30.5
TiO_2	0.52	0.55	0.56	0.53	0.56	0.49	0.52
Pu (nCi/g)	119	115	123	780	126	108	101
Total	**< 86.7**	**< 93.5**	**< 76.6**	**< 92.5**	**< 81.4**	**< 67.4**	**< 72.7**

Table 5. Analyzed Metal Phase Concentrations (wt %) for Each Test

Element	Nom-30	Nom-40	Nom-45	Nom-50	Nom-50 (75XPb)	Nom-50 (2XCl)	Nom-50 (2.5XNa)
Al	0.17	0.90	0.31	0.16	0.17	1.35	0.05
Ca	0.44	2.80	1.04	0.48	0.57	4.07	0.16
Ce	0.02	< 0.11	< 0.05	0.02	0.04		0.01
Cr	1.20	1.29	0.27	0.86	0.43	1.66	0.43
Fe	94.3	94.3	103.8	93.7	98.8	83.8	91.4
K	< 1.03	< 5.42	< 2.68	< 0.77	2.70		< 0.59
Mg	0.05	0.20	< 0.08	0.04	0.07	0.26	0.03
Mn	0.03	0.05	0.01	0.03	0.01	0.05	0.01
Ni	4.83	3.89	3.36	4.64	4.13		4.14
Pb	< 0.04	< 0.22	< 0.11	< 0.03	< 0.06	< 0.07	< 0.02
S	< 0.04	< 0.22	< 0.11	< 0.03	< 0.06	< 0.07	< 0.02
Si	0.29	1.27	0.85	0.33	0.53	1.34	0.13
Ti	0.01	0.05	0.02	0.01	0.01	0.05	0.01
Pu (nCi/g)	2.60	13.8	3.96	2.03	2.96	17.40	0.42
Total	**< 102**	**< 111**	**< 113**	**< 101**	**< 108**	**< 92.7**	**< 97.0**

Table 6. Analyzed Off-Gas Solid Phase Concentrations (wt %) for Each Test

Element	Nom-30	Nom-40	Nom-45	Nom-50	Nom-50 (75XPb)	Nom-50 (2XCl)	Nom-50 (2.5XNa)
Al	1.26	0.86	0.07	0.66	< 0.08	< 0.10	< 0.21
Ca	4.50	3.08	2.08	3.19	0.73	3.25	1.82
Ce	< 0.13	< 0.09	< 0.06	0.07	< 0.11		< 0.06
Cr	0.65	0.59	0.78	0.50	0.52	< 0.36	0.59
Fe	4.52	2.67	3.28	3.44	2.08	1.73	2.67
K	22.3	25.9		41.5			
Mg	0.52	0.52	0.42	0.31	< 0.18	< 0.48	< 0.30
Mn	0.19	0.18	0.22	0.11	0.18	< 0.20	0.21
Ni	0.24	0.26		0.41			
Pb	1.05	0.86	0.53	1.15	24.85		0.61
S	0.49	0.39	0.39	0.35	< 0.47	< 0.20	0.44
Si	10.8	9.3	8.7	4.7	6.5	8.5	8.7
Ti	0.04	0.03	0.02	0.03	0.02	0.01	0.02
Pu (nCi/g)	18.3	16.2	9.1	10.1	5.1	2.2	7.5
Total	**< 46.7**	**< 44.7**	**< 16.6**	**56.4**	**< 35.7**	**< 14.8**	**< 15.6**

Next, each of the phase concentrations, along with the total mass of each phase, was used to calculate the percentage of each element partitioned from the test feeds to a given phase. The equation used to calculate the partitioning of a given element, *i*, to a phase, *X*, for a given test is shown as follows:

$$\%\ \text{of}\ i\ \text{Partitioned to Phase}\ X\ =\ \frac{\text{Phase}\ X\ \text{Mass}\ *\ \text{Phase}\ X\ \text{Concentration of}\ i}{\text{Feed Mass}\ *\ \text{Feed Concentration of}\ i}$$

The glass, metal, and off-gas phase partitioning totals for each element are expected to sum to 100%, indicating that all of the mass was accounted for. Table 7 compiles the partitioning values for each test.

Most of the elements in Table 7 show glass, metal, and off-gas partitioning totals (or total mass recoveries) around 100%, within the stated error ranges. The glass phase partitioning values contribute the largest portion to the mass recovery error, primarily because of the relatively larger mass of that phase. Note that sampling error is not accounted for in the values in Table 7. Sampling error is expected to be significant for the glass data because of the potential inhomogeneity of those samples. For example, the cerium glass phase partitioning values were nearly 100% for all of the tests, except for the Nom-45 and high-sodium Nom-50 tests. These two tests had glass phase partitioning values for cerium of approximately 50%, with no corresponding increases in either the metal or off-gas. A similar case is suspected for the Nom-50 glass phase partitioning value for plutonium. This value was 865%. Each of the other tests had glass phase recoveries for plutonium on the order of 100%, indicating a nonhomogeneous Nom-50 glass sample.

The glass phase partitioning values for lead, as shown in Table 7, were below the analytical instrument detection levels for each test. These values resulted in total mass recoveries ranging between <55% and <148%. Nevertheless, the corresponding off-gas values were above detection levels for most of the tests and are expected to be useful despite the poor total mass recoveries. Note that no off-gas partitioning values for lead are shown for the high-chloride Nom-50 test in Table 7. That test followed the high-lead Nom-50 test which left residual lead in the furnace off-gas system.

The previously discussed silica errors are again revealed in Table 7. Here, most of the tests show total recoveries of silica between 47% and 91%. Calcium, the other predominant specie in the glass, has total recoveries near 100% for each test. This further supports a suspected low bias in the silica values. This bias is assumed to primarily apply to the glass phase values but may extend to the other phases as well.

The total mass recoveries for the metal phases of each test were nearly 100%, except for iron and chromium in the Nom-30 test. Table 7 shows total mass recoveries for those elements of 74% each. These low recoveries are assumed to have occurred because not all the metal from the Nom-30 test was retrieved.

Table 7. Phase Partitioning Values (Percent) for Each Test

	Nom-30				Nom-40				Nom-45				Nom-50			
Phase	**Glass**	**Metal**	**Gas**	**Total**	**Glass**	**Metal**	**Gas**	**Total**	**Glass**	**Metal**	**Gas**	**Total**	**Glass**	**Metal**	**Gas**	**Total**
Error	± 14%	± 14%	± 20%		± 14%	± 14%	± 31%		± 14%	± 14%	± 27%		± 14%	± 14%	± 14%	
Al	118	0.79	1.9	121 ± 17	104	5.6	1.5	111 ± 15	109	1.3	0.1	111 ± 15	106	0.68	0.32	107 ± 15
Ca	98	0.79	2.6	101 ± 14	96	6.1	1.9	104 ± 14	93	1.5	0.8	96 ± 13	95	0.64	0.50	96 ± 13
Ce	116	1.3	< 2.3	< 120 ± 16	102	< 8.6	< 2.1	< 113 ± 15	50	< 3.0	< 0.9	< 54 ± 7	100	1.0	0.46	101 ± 14
Cr	55	16	2.8	74 ± 8	64	29	3.8	97 ± 10	57	4.7	3.6	65 ± 8	59	17	1.2	77 ± 9
Fe	1.3	72	1.1	74 ± 10	1.2	121	1.0	123 ± 17	1.6	102	0.8	104 ± 14	2.8	102	0.44	105 ± 14
K	7.3	< 10	75	< 92 ± 15	< 8.9	< 80	108	< 196 ± 35		< 28		± 4	16	< 8.0	51	< 75 ± 7
Mg	96	1.1	4.0	102 ± 14	89	6.4	4.7	100 ± 13	75	< 1.8	2.4	< 79 ± 11	96	0.88	0.77	98 ± 14
Mn	76	6.9	13	96 ± 11	53	15	15	83 ± 9	74	2.8	12	89 ± 11	85	5.8	3.0	94 ± 12
Ni	2.5	82	1.3	86 ± 12	4.2	114	2.1	121 ± 16		77		± 11	5.0	119	1.2	125 ± 17
Pb	< 15	< 6	46	< 67 ± 9	< 37	< 50	56	< 144 ± 19	< 65	< 19	25	< 109 ± 12	< 59	< 6	27	< 93 ± 9
S	34	< 4.1	16	< 54 ± 6	48	< 37	19	< 105 ± 10	73	< 14.4	13	< 101 ± 11	92	< 4.6	6.2	< 103 ± 13
Si	75	0.44	5.4	81 ± 11	82	2.3	4.8	89 ± 12	61	1.0	2.7	64 ± 9	90	0.37	0.62	91 ± 13
Ti	100	1.1	1.4	103 ± 14	93	6.2	1.2	100 ± 13	96	1.4	0.5	98 ± 14	91	0.72	0.29	92 ± 13
Pu	102	0.76	1.8	105 ± 14	106	5.8	1.9	114 ± 15	127	1.2	0.7	129 ± 18	865	0.61	0.35	866 ± 122

	Nom-50 (75XPb)				Nom-50 (2XCl)				Nom-50 (2.5XNa)			
	Glass	**Metal**	**Gas**	**Total**	**Glass**	**Metal**	**Gas**	**Total**	**Glass**	**Metal**	**Gas**	**Total**
Error (%)	± 14%	± 14%	± 27%		± 14%	± 14%	± 33%		± 14%	± 14%	± 36%	
Al	87	0.74	< 0.22	< 88 ± 12	104	5.9	< 0.19	< 110 ± 15	89	0.20	< 0.37	< 89 ± 13
Ca	102	0.81	0.67	103 ± 14	88	5.7	1.9	96 ± 13	94	0.22	1.0	95 ± 13
Ce	77	2.2	< 4.0	< 83 ± 11					44	0.72	< 1.5	< 46 ± 6
Cr	76	9.2	7.1	92 ± 11	32	35	< 3.2	< 70 ± 7	78	8.4	4.9	91 ± 11
Fe	2.1	114	1.5	118 ± 16	1.3	96	0.8	98 ± 14	2.9	98	1.2	102 ± 14
K		30.0								< 6.0		
Mg	90	1.6	< 2.7	< 94 ± 13	81	6.0	< 4.5	< 91 ± 12	82	0.57	< 2.7	< 85 ± 12
Mn	97	2.7	27.9	128 ± 16	58	13	< 19	< 90 ± 11	88	2.1	20	111 ± 14
Ni		113								104		
Pb	< 3.0	< 0.19	52	< 55 ± 14	< 43	< 15			< 92	< 5	52	< 148 ± 23
S	< 147	< 9.6	< 48.9	< 206 ± 25	55	< 11	< 13	< 79 ± 9	< 68	< 3.5	28	< 99 ± 14
Si	68	0.63	5.0	74 ± 10	40	1.6	4.2	46 ± 6	61	0.14	4.1	65 ± 9
Ti	96	0.55	0.87	97 ± 14	77	4.0	0.39	81 ± 11	91	0.87	0.64	92 ± 13
Pu	132	0.90	1.0	134 ± 19	105	5.2	0.27	111 ± 15	110	0.12	0.9	111 ± 16

Partitioning Analysis

The data presented in Table 7 can next be plotted to compare how individual elements partitioned between phases for each test. As discussed previously, the majority of the suspected error in the data lies with the glass analytical values. Therefore, the focus will be mostly on the metal and off-gas partitioning values. Figures 5 and 6 show the metal phase partitioning values for each test. Note that the values in Table 7, which were below the analytical equipment detection levels, were omitted from these plots.

Figure 5 shows that between 70% and 120% of the iron and nickel partitioned to the metal phase for each test. The closeness to 100% of these partitioning values, with associated uncertainties of 14%, indicates that nearly all of these two elements partitioned to the metal phases. Additionally, significant amounts, over 10%, of potassium, chromium, lead, and manganese partitioned to the metal phase for most tests. The furnace temperatures and feed reducing potentials govern whether certain elements reduce to metal, from an oxide or salt, or oxidize from their metallic form. The elements shown in Figure 5 are commonly reduced to metals in conditions like those in the tests discussed here (Soelberg et al. 1994). No clear trends are evident between the partitioning of any of these elements to the metal phase and feed composition change. The Nom-40 test did produce a higher potassium partitioning value compared to the Nom-30 test. However, this comparison cannot be used to substantiate a relationship to organic content.

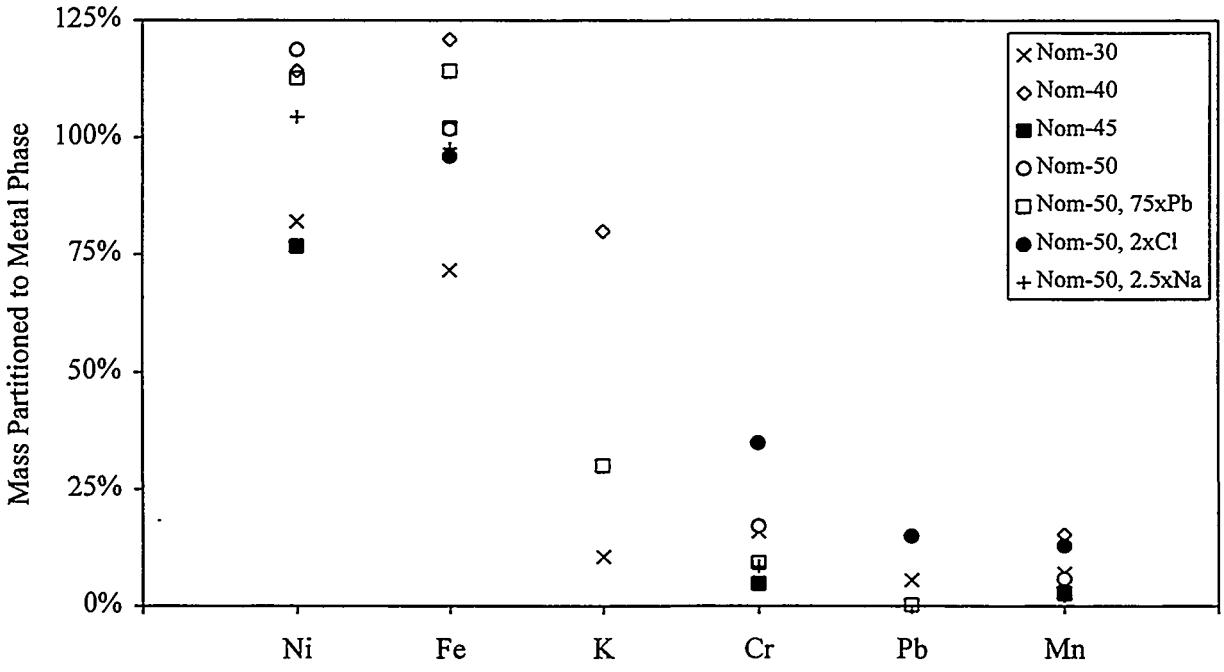

Figure 5. Metal Phase Partitioning Values for Each Test (Part 1)

Figure 6 shows the elements that commonly form, or remain as, oxides. As oxides these elements typically migrate to the glass phases of melts. The low metal phase partitioning values of these elements, less than 10%, support this generalization.

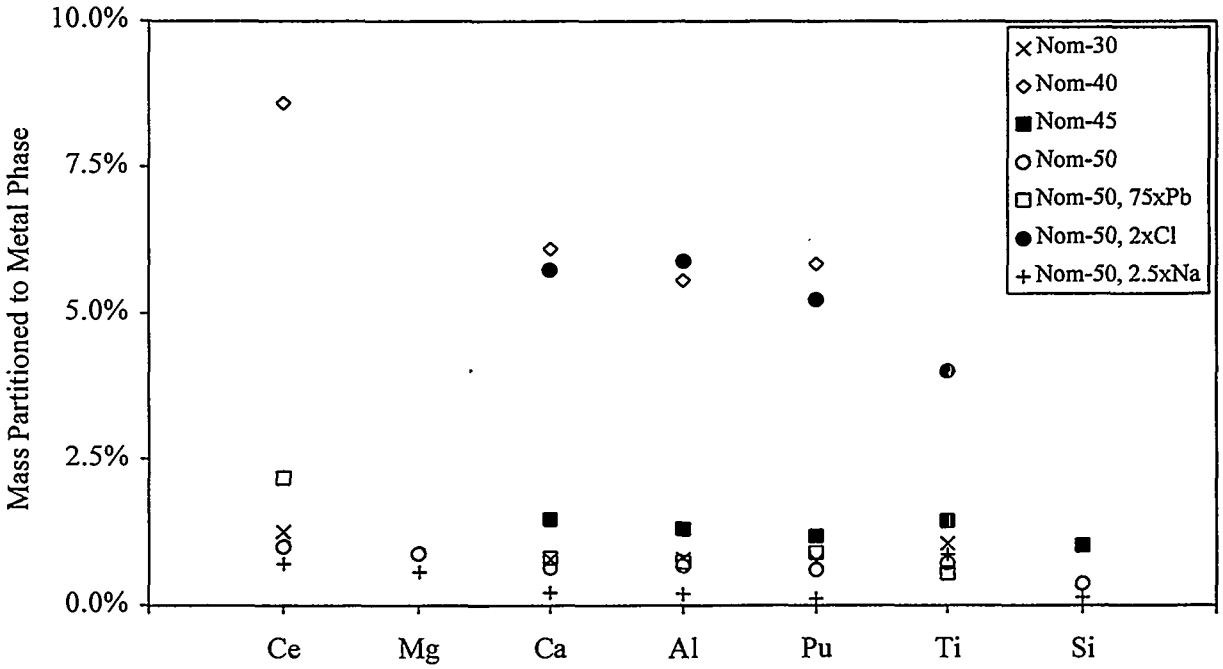

Figure 6. Metal Phase Partitioning Values for Each Test (Part 2)

Each of the expected-oxide elements in Figure 6 appears to have nearly consistent metal phase partitioning values for a given test. Each of the tests represented in this figure, except for the Nom-40 and high-chloride Nom-50 tests, have metal phase partitioning values of less than 2%. The Nom-40 and high-chloride Nom-50 tests have partitioning values between 4% and 8%. Recall that the Nom-40 composition had a mid-range organic content, between that for Nom-30 and Nom-45. Therefore, the increased metal phase partitioning values in Figure 6 for Nom-40, over those for both Nom-30 and Nom-45, indicate that the feed composition did not cause the difference. Instead, the consistent increase in metal phase partitioning for the Nom-40 and high-chloride Nom-50 tests suggests that glass contaminated the metal samples from those two tests. Indeed, residual glass remained in some of the samples as a result of the metal sampling procedure. A metal stream produced from a larger, continuously poured system is not expected to be susceptible to this type of glass contamination in the metal phase.

Since the primary metal phase partitioning mechanism for the elements in Figure 6 is suspected to be glass contamination, for at least two of the tests the data were further compared to determine if dissolution of any of the elements, specifically plutonium, into the metal phase could be ascertained. As part of these comparisons the metal phase partitioning values for calcium, aluminum, and titanium for each test were plotted against the corresponding values for plutonium. This plot is shown in Figure 7. The dashed line in this figure represents a one-to-one partitioning relationship between plutonium and the other constituents, indicative of a shared metal phase partitioning mechanism.

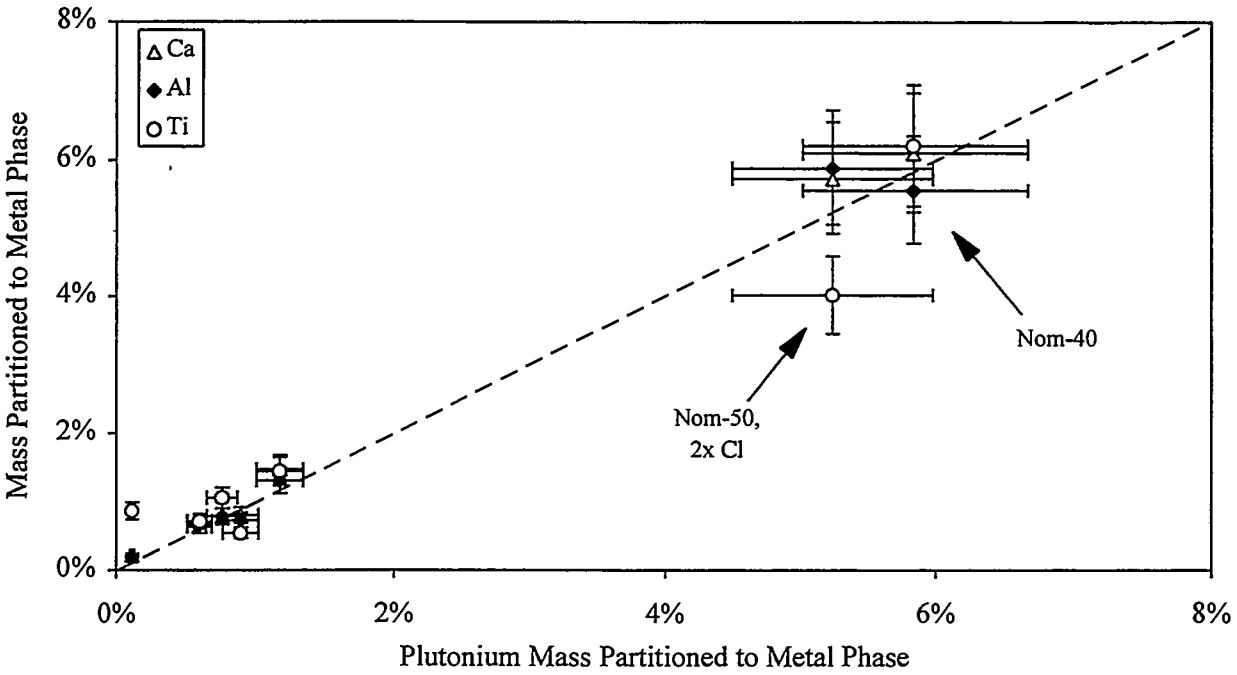

Figure 7. Metal Phase Partitioning Values of Suspected Oxides Versus Plutonium

Indeed, each of the data points in Figure 7 appear to fall on or near the dashed line shown, indicating that the metal phase partitioning affinity of plutonium is near that for the other three elements for each test. Since these data further support a constant partitioning of each suspected oxide, it can be concluded that plutonium partitioning to the metal phases of each test corresponded only to levels proportional to glass contamination. Note that the plutonium-titanium data points in Figure 7 are generally more scattered than the others with two points, from the high-chloride and high-sodium Nom-50 tests, lying significantly outside their error ranges. To better quantify this scatter, linear regressions of each of the data point sets in Figure 7 were calculated. Table 8 shows the results of those regressions.

Table 8. Linear Regression Parameters for Metal Partitioning Data Comparisons

Parameter	Al Versus Pu	Ca Versus Pu	Ti Versus Pu
Slope	1.02	1.06	0.87
Y Intercept	0.0003	0.0003	0.002
r^2	0.99	1.00	0.93

Table 8 shows that the aluminum-plutonium and calcium-plutonium data points more closely fit a one-to-one relationship than the titanium-plutonium data points. The titanium analytical data are the primary cause for the scattered titanium-plutonium data points. Sampling and analytical errors are not considered to be a significant factor. More likely is the possibility of some alloying of metallic titanium into the metal phase.

Next, the off-gas partitioning values for each element in Table 7 were compared. Plots of these values are shown in Figures 8 and 9.

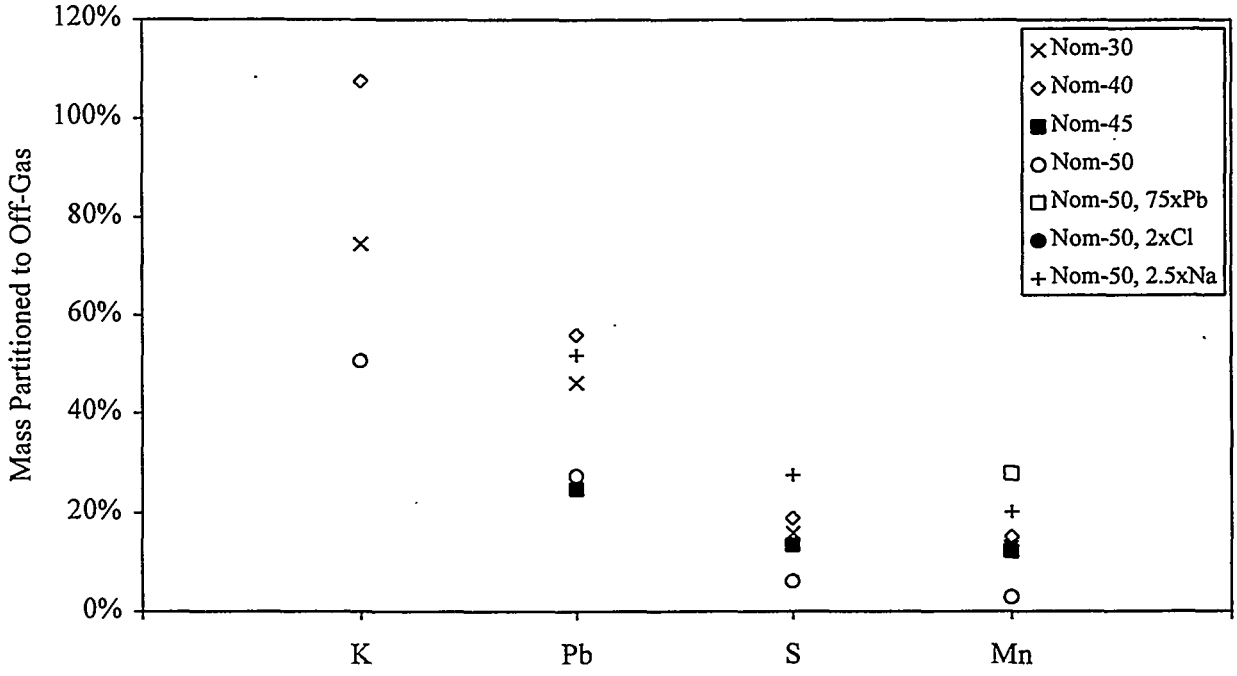

Figure 8. Off-gas Phase Partitioning Values for Each Test (Part 1)

Figure 8 shows the elements with the highest off-gas partitioning values. The potassium and lead values range between 25% and 100% for each test shown. The Nom-40 test shows higher partitioning values for all four of the elements compared to either the Nom-30 or Nom-50 tests which had, correspondingly, lower and higher organic contents. This indicates that the average glass temperature of each test and the extent the glass was covered with feed were the primary mechanisms for partitioning of these highly volatile constituents to the off-gas, not the surrogate composition.

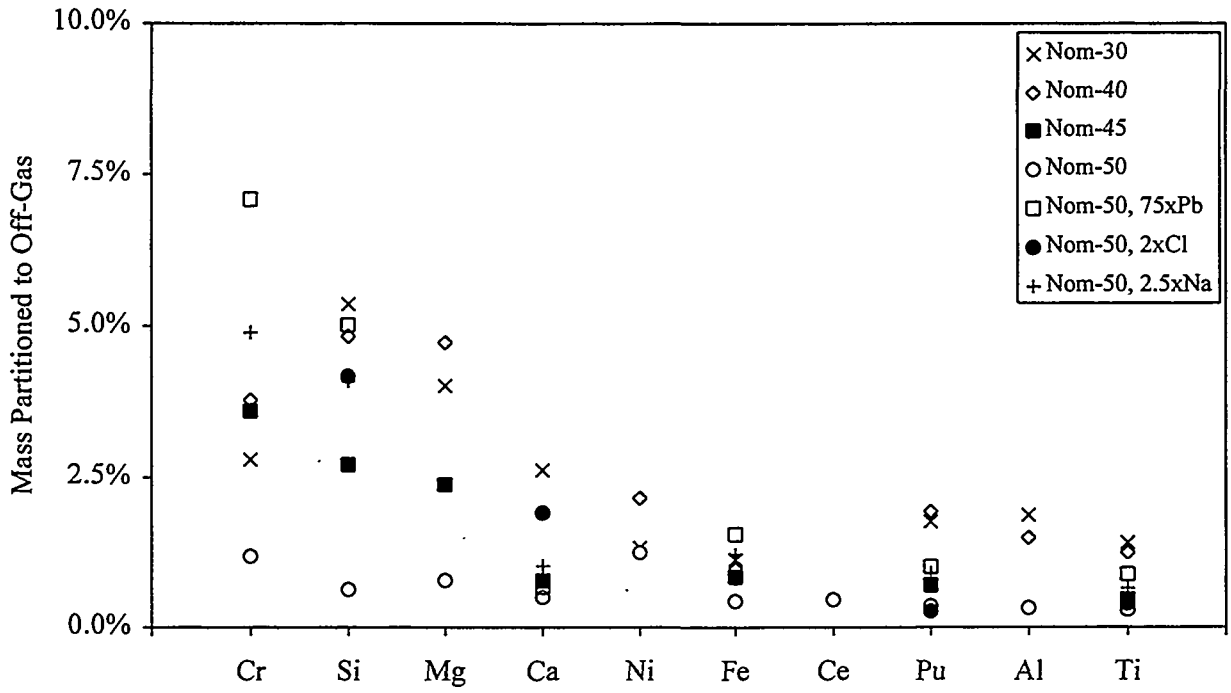

Figure 9. Off-gas Phase Partitioning Values for Each Test (Part 2)

Figure 9 plots the elements with off-gas partitioning values of less than 10%. In this plot the highest values are for chromium, silicon, and magnesium. The remaining elements all have off-gas partitioning values of below 3%. Except for iron and nickel, those elements are expected to be in their oxide forms since they were predominantly soil constituents and are not easily reduced to their metal forms. Since the boiling points of the oxide forms of each of these elements is above 2400°C, the expected off-gas partitioning mechanism for those elements is entrainment from the feed stream. Entrainment refers to material that was not volatilized during processing, but was carried directly into the off-gas. Typically, entrainment varies with a given furnace since its size, off-gas flow rates, and respective feed and off-gas line placements all can contribute to the amount of feed swept into the off-gas lines (Whyatt et al. 1996). Conversely, volatility is more dependent on the furnace operating temperature and the extent the glass is covered with feed material at steady-state operating conditions.

To further identify the off-gas partitioning mechanisms for the last seven elements in Figure 9, particularly for plutonium, the individual off-gas partitioning values for calcium, aluminum, and titanium were plotted against those for plutonium. This plot is shown in Figure 10. Note that nickel and iron were not plotted since they were shown not to share the same partitioning mechanism as plutonium to the metal phase. Additionally, cerium was omitted from the plot as all its off-gas partitioning values, except for the value from the Nom-50 test, were based on values below analytical detection limits.

Figure 10 shows a nearly one-to-one relationship between plutonium off-gas partitioning and that for calcium, aluminum, and titanium, except for the calcium values from the Nom-30 test and the high-chloride Nom-50 test. Those two points correspond to the two feeds with the highest chloride content

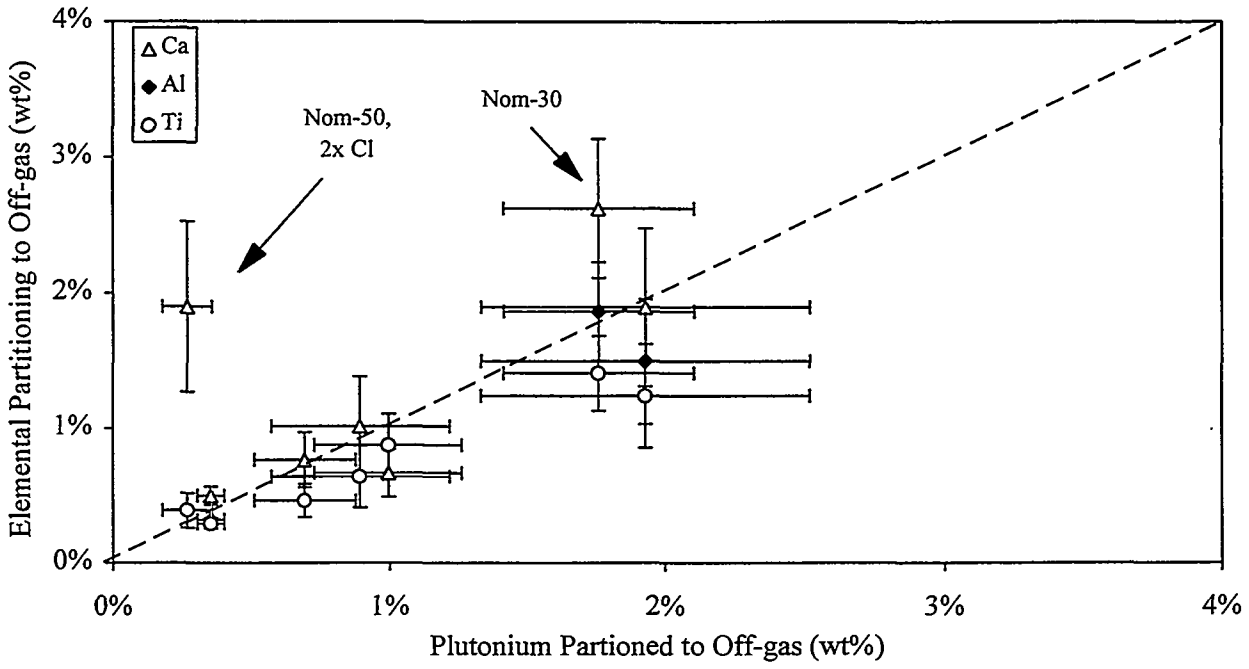

Figure 10. Plutonium Off-gas Phase Partitioning Compared with That for Low-Volatility Oxides

(from PVC) in their starting materials. Calcium chloride has a higher vapor pressure, at a given temperature, than calcium oxide. Therefore, the formation of calcium chloride could have led to the higher measured off-gas partitioning values for those two tests. Interestingly, plutonium chloride also has higher vapor pressures than its oxide form, yet no increase in plutonium partitioning is evident for the high-chloride feeds. The higher mass of calcium in the feeds, compared to plutonium, may have resulted in this difference.

The off-gas partitioning relationships in Figure 10 support that each of the elements shared the same mechanism of mass transfer to the off-gas system, except for calcium. The vapor pressures of each of the oxides of aluminum, titanium, and plutonium are similar but differ enough such that each would have partitioned differently if volatility were the primary mechanism for transfer to the off-gas (TPRC 1967). Therefore, it is assumed that entrainment was the primary mechanism for the off-gas partitioning of each of these elements. Note that a linear regression of just the plutonium-titanium data points in Figure 10 gives a slope of 0.64 (r^2 of 0.93) and a y intercept near zero. This regression would indicate that plutonium had an average off-gas partitioning around 30% higher than titanium. However, when the data error is considered this trend is difficult to substantiate. Note that no regression trends were calculated for the aluminum-plutonium off-gas partitioning values since only a few of those values were above analytical detection levels. Still, based on the few data points available, aluminum, as an oxide, off-gas partitioning values are expected to trend closely with those for plutonium oxide.

Conclusions

Each of the SDA buried waste surrogates produced separable glassy and metallic phases for each blend tested, however, furnace power levels were found to fluctuate more with blends having higher organic contents. An organic content corresponding to a Nom-50 composition was determined to be the highest achievable before power fluctuations led to unacceptable operating conditions in the test system.

Hazardous metal behavior data was obtained for both chromium and lead. Less than one half of the chromium and one quarter of the lead from each surrogate blend tested was found to partition to the metal phases. Additionally, each test showed less than 8% of the chromium and between 25% and 60% of the lead partitioned to the off-gas. No individual surrogate blend variation was found to have directly impacted these values. Instead, indirect impacts from differing slag temperatures or feed coverage of the glass are suspected.

Similarly, none of the waste surrogate variations tested was found to have a singular impact on plutonium partitioning to the metal or off-gas solids phases. The metal phases from each test had near-constant partitioning values for calcium, aluminum, plutonium, and titanium, indicating that they were present in glass inclusions or residual glass on the metal samples. The method for sampling the metal was amenable to this type of contamination. Still, the lowest feed-to-metal phase partitioning value measured for plutonium was 0.1%. This value may represent a realistic plutonium metal-phase partitioning value, even for larger furnaces which are less susceptible to glass inclusions in the metals produced. The feed-to-off-gas solids phase partitioning values for each element also showed near-constant values for calcium, aluminum, plutonium, and titanium for each test. The low vapor pressures of each of their oxide forms suggest entrainment, not volatility, to be the primary mechanism for their transfer to the off-gas. Based on this, the entrainment behavior of a given furnace, operating at similar temperatures, can be used to estimate plutonium off-gas partitioning. Additionally, low volatility elements, like aluminum and titanium, may act as reasonable plutonium surrogates in nonradioactive arc furnace testing.

References

Bonnenberg RW, RE Heard, LM Milam, LR Watson. 1993. *Buried Waste Integrated Demonstration FY-93 Deployment Plan.* EGG-WTD-10539, EG&G Idaho, Inc., Idaho Falls, Idaho.

Geimer R, T Hertzler, R Gillins, GL Anderson. 1992. *Assessment of Incineration and Melting Technologies for RWMC Buried Waste.* EGG-WTD-10035, EG&G Idaho, Inc., Idaho Falls, Idaho.

Mayberry JL, WJ Quapp, F Feizollahi, JC DelSignore. 1991. *Preliminary Systems Design Study Assessment Report.* EGG-WTD-9594, EG&G Idaho, Inc., Idaho Falls, Idaho.

Nickelson DF, J Luey, RA Callow. 1992. *ISV Technology Development Plan for Buried Waste.* EGG-WTD-10325, EG&G Idaho, Inc., Idaho Falls, Idaho.

Soelberg NR, AG Chambers, GL Anderson, LL Oden, WK O'Conner, PC Turner. 1994. *Arc Melter Demonstration Baseline Test Results.* EGG-WTD-11138, EG&G Idaho, Inc., Idaho Falls, Idaho.

Thermophysical Properties Research Center (TPRC). 1967. *Thermophysical Properties of High Temperature Solid Materials. Vol. 4, Parts 1 and 2.* Purdue University, West Lafayette, Indiana.

Whyatt GA, JW Shade, GE Stegen. 1996. *Volatility and Entrainment of Feed Components and Product Glass Characteristics During Pilot-Scale Vitrification of Simulated Hanford Site Low-Level Waste.* WHC-SA-3093-FP, Westinghouse Hanford Company, Richland, Washington.

Appendix A

Test Operating Data

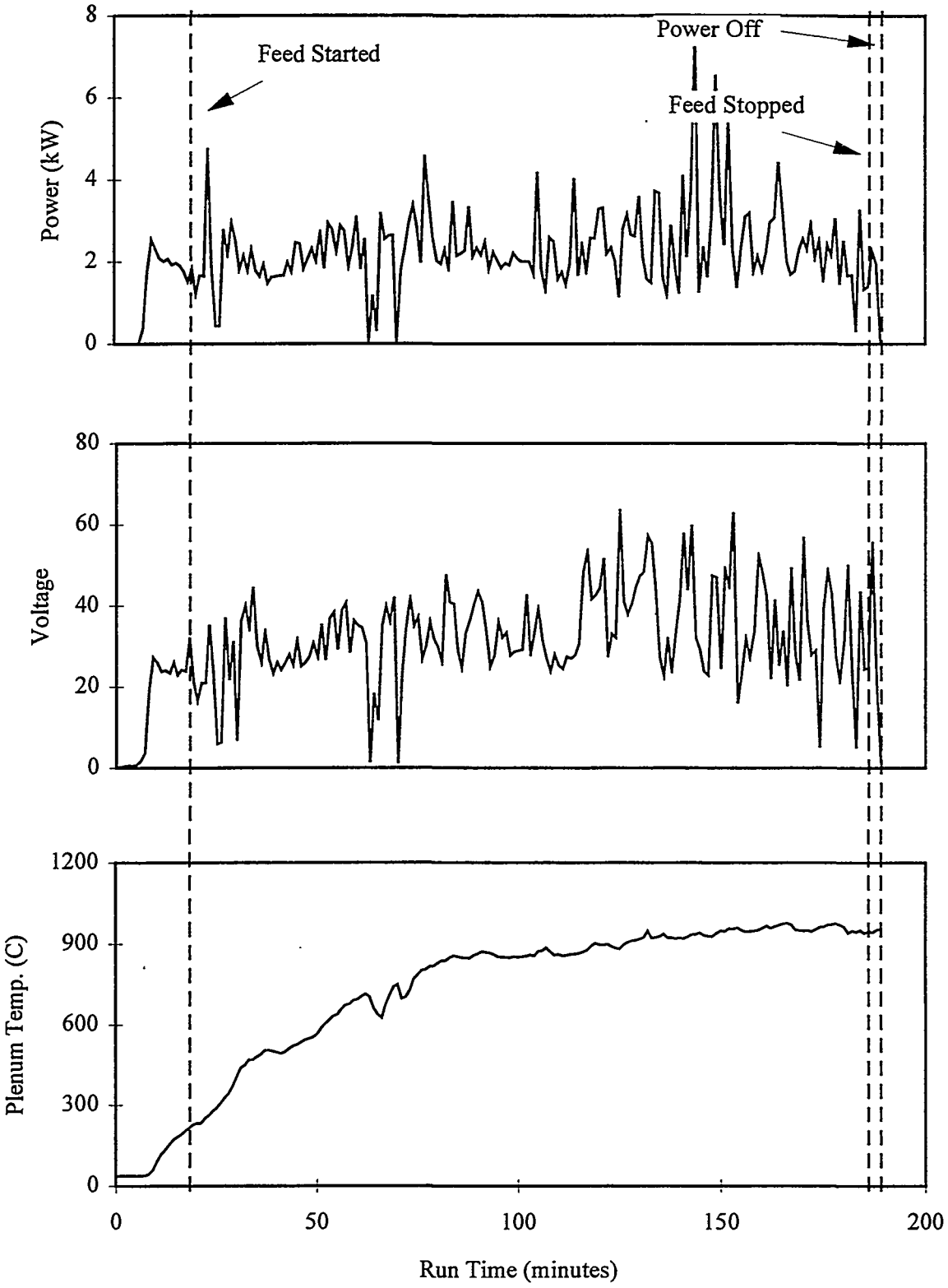

Figure A.1. Nom-30 Test Power and Temperature Data

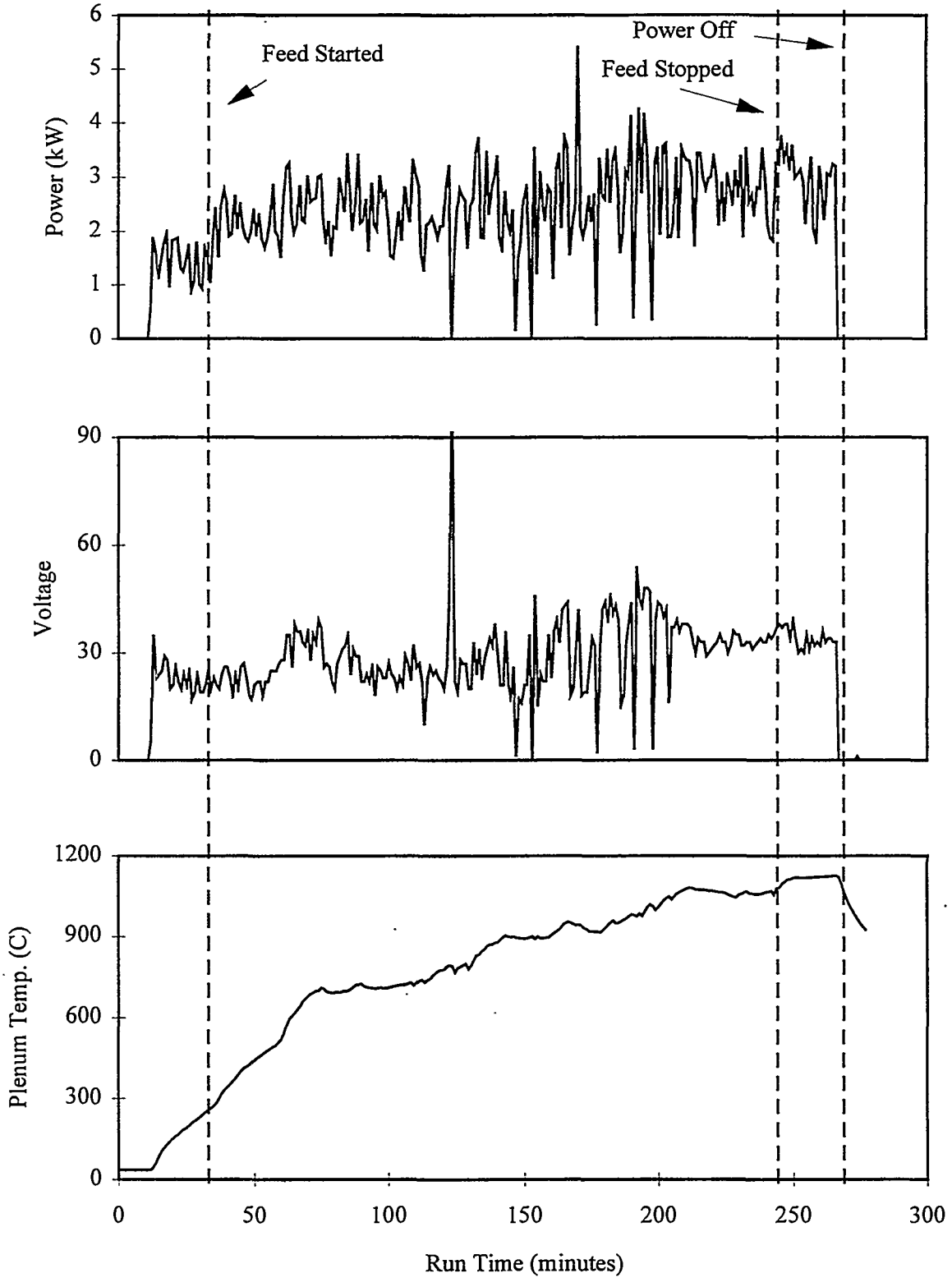

Figure A.2. Nom-40 Test Power and Temperature Data

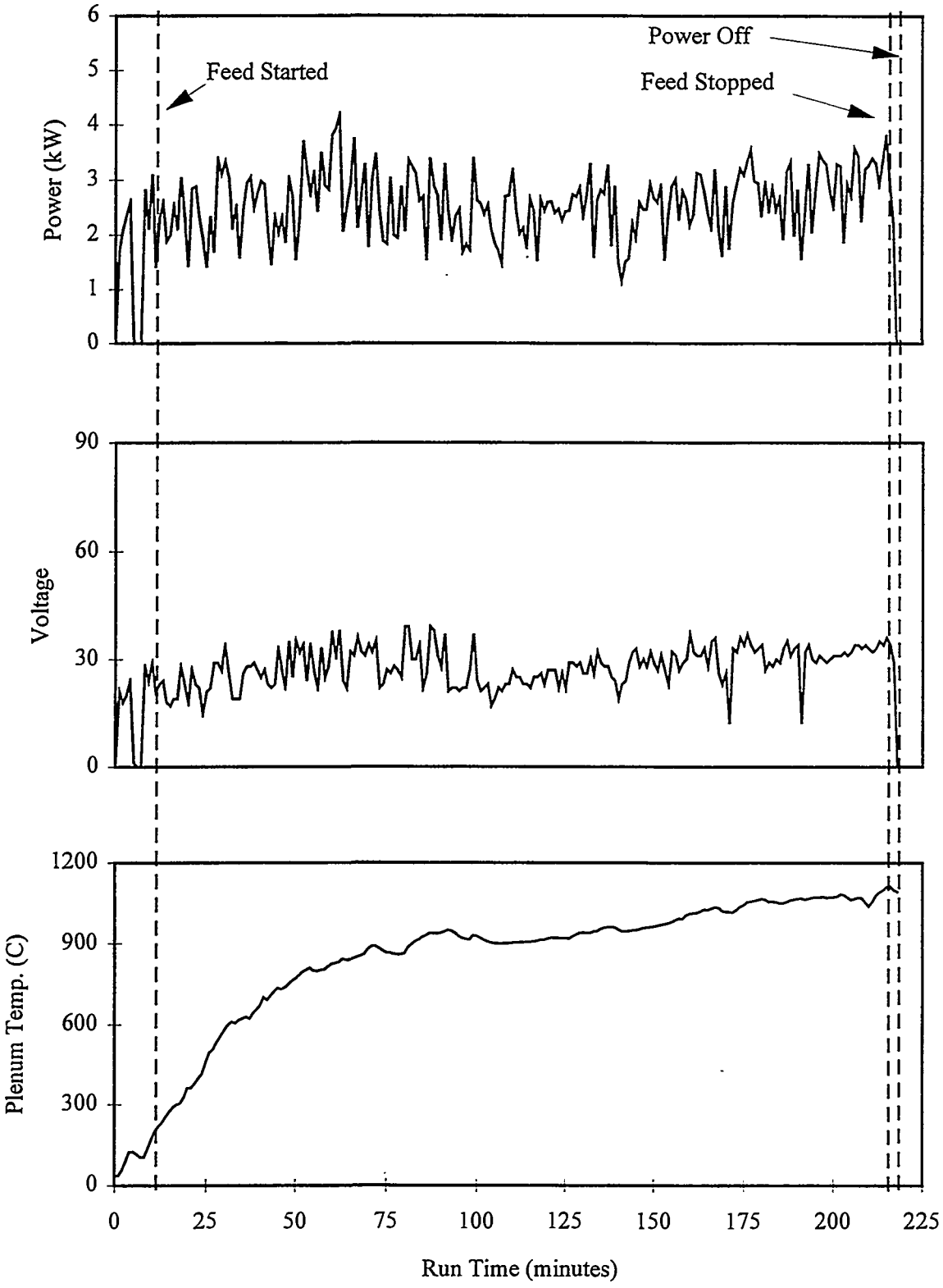

Figure A.3. Nom-45 Test Power and Temperature Data

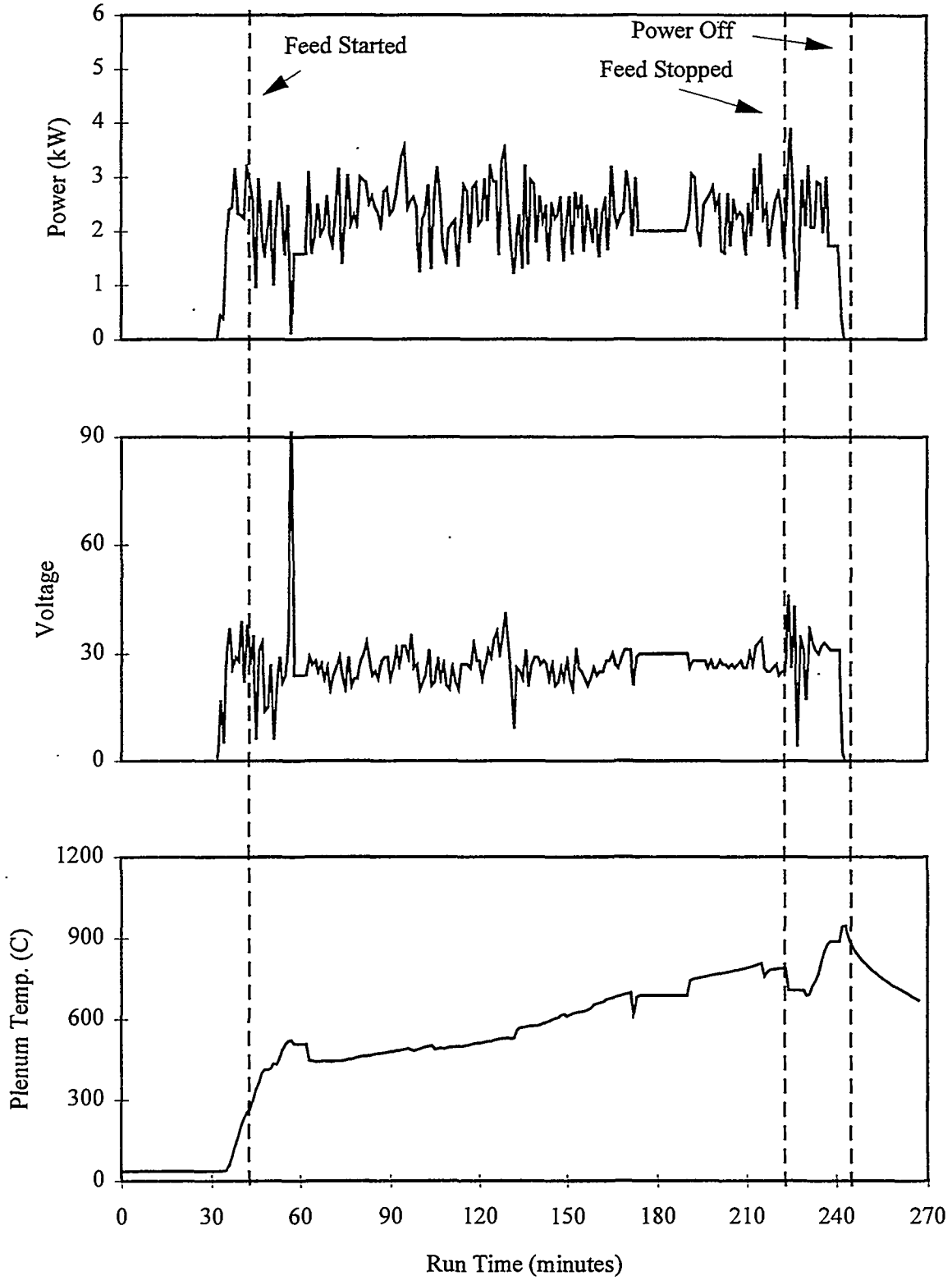

Figure A.4. Nom-50 Test Power and Temperature Data

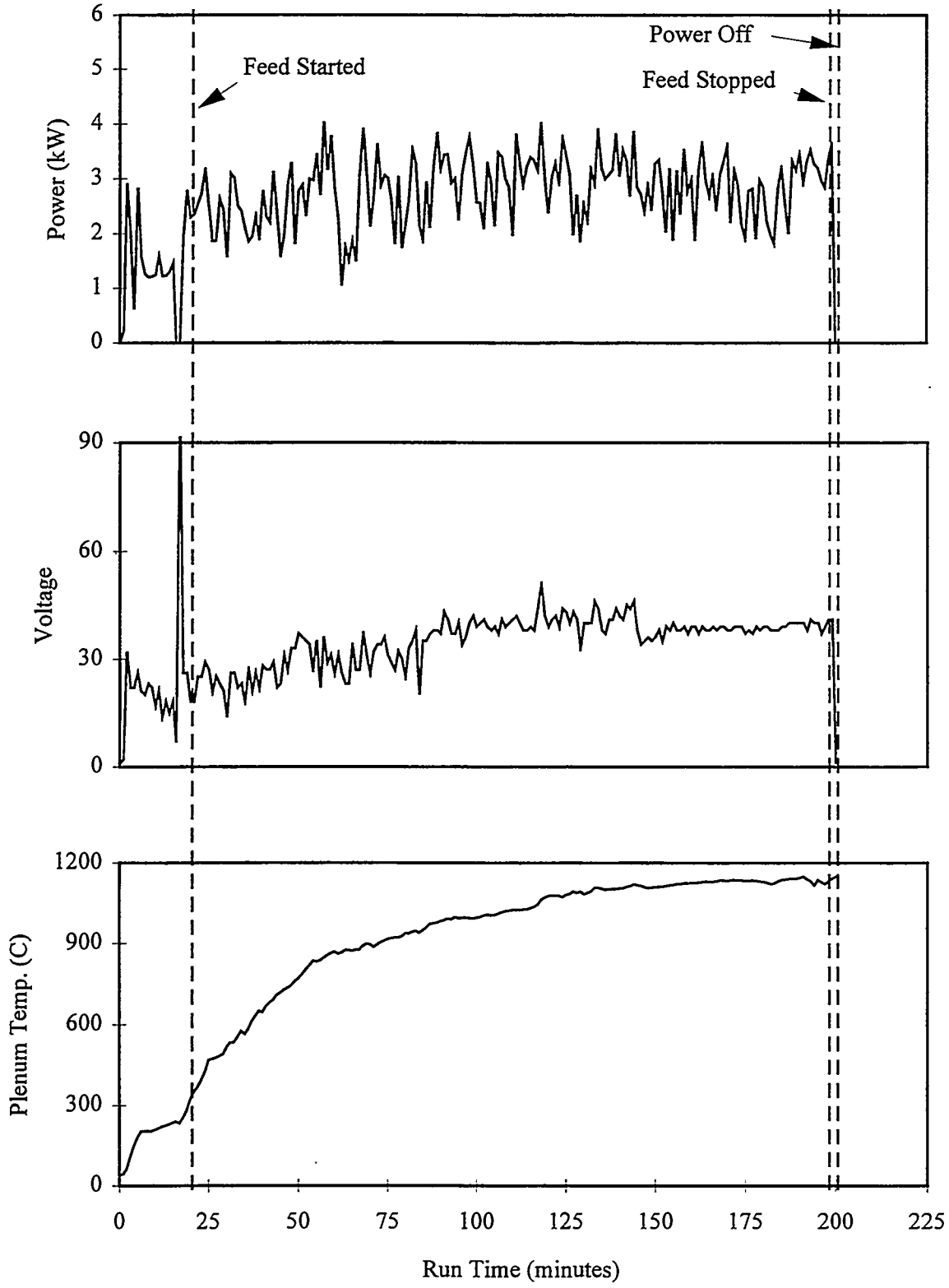

Figure A.5. Nom-50 (High Lead) Test Power and Temperature Data

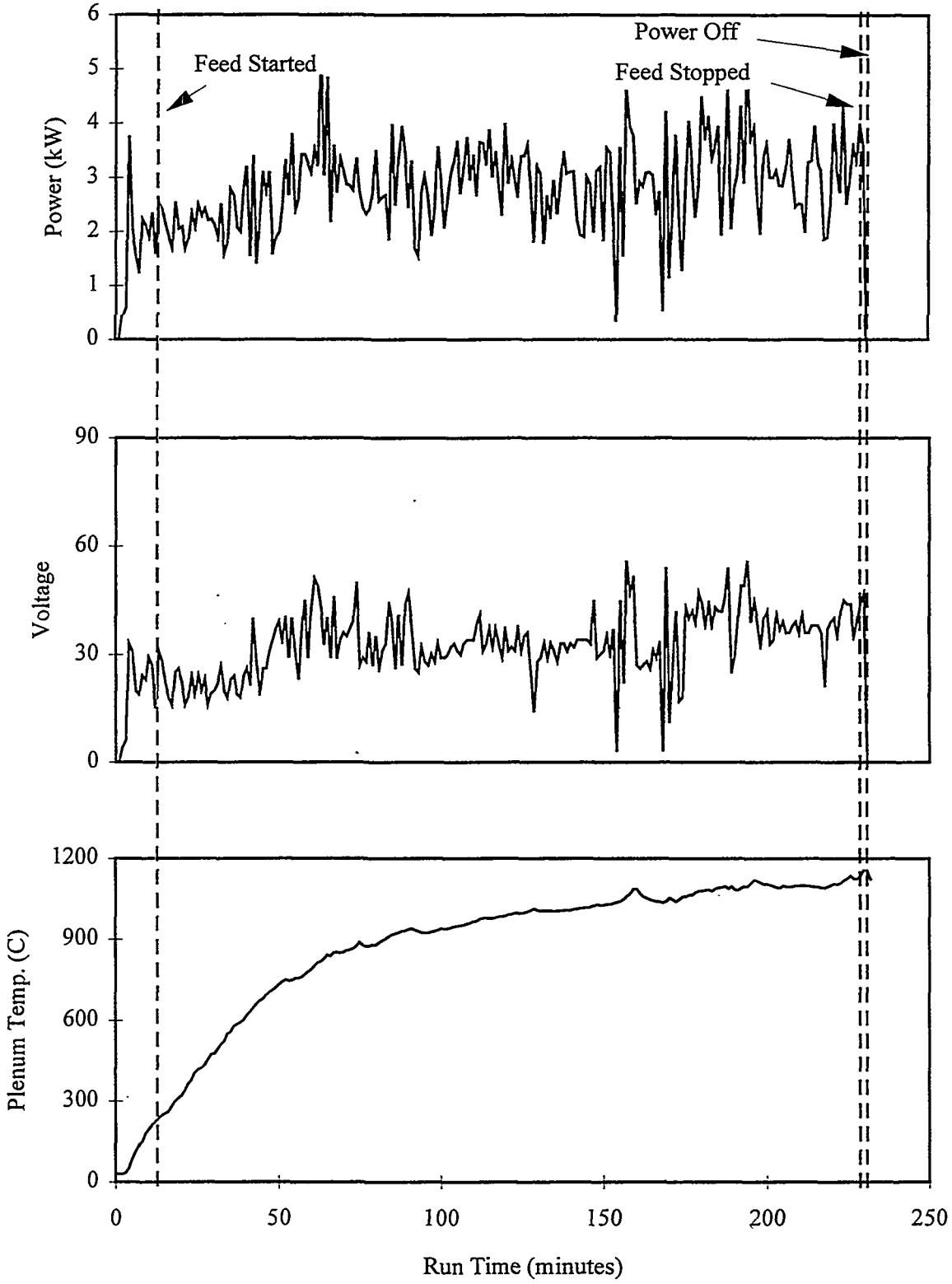

Figure A.6. Nom-50 (High Chloride) Test Power and Temperature Data

Distribution

No. of
Copies

OFFSITE

2 DOE/Office of Scientific and Technical Information

2 U.S. Department of Energy
Germantown
19901 Germantown Rd.
Germantown, MD 20874-1290
ATTN: J. Bassi
C.B. Purdy

7 Idaho National Environmental and Engineering Laboratory
850 Energy Drive
Idaho Falls, ID 83401
ATTN: G. L. Anderson, MS-3710
M. J. Connolly, MS-3875
D. Gombert, MS-3875
J. D. Herzog, MS-3875
M. R. Martin, MS-4201
N. R. Soelberg, MS-3625
W. St. Michel, MS-3875

R. K. Nakaoka
Los Alamos National Laboratory
PO Box 1663
MS-E517
Los Alamos, NM 87545

No. of
Copies

2 Savannah River Ecology Laboratory
Savannah River Site, Building 737A
Aiken, SC 29802
ATTN: N. M. Askew
J. W. Congdon

4 MWFA Program Office
PO Box 1625
MS-3875
Idaho Falls, ID 83415
ATTN: R. J. Kimmel
J. H. Koltz
W. A. Owca
L. C. Thomas

ONSITE

3 DOE Richland Operations Office

J. P. Hanson	K8-50
R. A. Pressentin	K8-50
J. J. Waring	S7-55

48 Pacific Northwest National Laboratory

W. F. Bonner	(25)	K9-14
M. L. Elliott		P7-41
C. J. Freeman	(12)	P7-41
D. A. Lamar		P7-41
R. A. Merrill		P7-41
D. K. Seiler		P7-41
Information Release	(7)	